Available online at www.sciencedirect.com
ScienceDirect
Journal of Catalysis 249 (2007) 311–317
JOURNAL OF CATALYSIS
www.elsevier.com/locate/jcat

In situ surface-enhanced IR absorption spectroscopy on the adsorption and reduction of nitric oxide at ruthenium electrode

Yan-Gang Yan, Bei-Bei Huang, Jin-Yi Wang, Hui-Feng Wang, Wen-Bin Cai *

Shanghai Key Laboratory for Molecular Catalysis and Innovative Materials and Department of Chemistry, Fudan University, Shanghai 200433, PR China

Received 28 February 2007; revised 9 April 2007; accepted 6 May 2007

Available online 19 June 2007

Abstract

Real-time attenuated total-reflection surface-enhanced infrared absorption spectroscopy (ATR-SEIRAS), in conjunction to cyclic voltammetry, was applied to investigate the adsorption and reduction of nitric oxide at Ru electrode in acidic solutions. For a NO-predosed Ru electrode, only one band located at 1840–1874 cm^{-1} was detected in 0.1 M $HClO_4$, attributable to atop NO coadsorbed with oxygen-containing species [designated ν_2(O)–NO species]. For a Ru electrode in 0.1 M $HClO_4$ containing 20 mM $NaNO_2$, two IR bands were observed at 1850–1886 cm^{-1} and 1740–1790 cm^{-1}. The former, predominant at relatively high potentials, is ascribable to the ν_2(O)–NO species; the latter, to atop NO adsorbed on nominal Ru sites at relatively low potentials (designated ν_2-NO species). In addition, a very weak band at 1520–1578 cm^{-1} may be assigned to multicoordinated NO coadsorbed with oxygen-containing species. The real-time spectral results suggest that the reduction of NO molecules and the coadsorbed oxygen-containing species proceed simultaneously rather than separately.

Keywords: Surface-enhanced infrared absorption spectroscopy; Nitric oxide; Adsorption and reduction; Ruthenium electrode

1. Introduction

The adsorption and reduction of NO on transition metal electrodes have received extensive attention due to its scientific and technological significance. Practically, it is related to electrocatalytic removal of NO_3^-, NO_2^-, and NO in wastewater treatment [1] and to the electrocatalytic production of N_2O, NH_3, and NH_2OH from nitrate solutions [2–4]. Fundamentally, NO has been used as a model molecule by surface electrochemists to probe the effects of electronic properties of metal electrodes on adlayer structures [5,6], as well as their correlations with the corresponding UHV measurements [7–13] and the results from ab initio density functional calculations [14].

Pt-group metals are known to be excellent catalysts for the reduction of NO_3^-, NO_2^-, and NO [15–19]. The adsorption and reduction of NO on Pt, Pd, Rh, and Ir electrodes have been studied intensively with conventional infrared absorption reflection spectroscopy (IRAS) by groups from Alicante [20–23], Purdue [5,6,24,25], and Eindhoven [26,27]. These studies have arrived at a consensus that vibrational frequencies depend on the properties of metals, surface coverage, and applied electrode potentials. The reduction of both adsorbed NO and solution NO on Pt, Pd, Rh, and Ru electrodes also has been studied by Koper et al. [15] using differential electrochemical mass spectroscopy (DEMS) in combination with rotating disk electrode (RDE) measurements. They found that for reduction of solution NO, all metals showed a high selectivity toward the production of N_2O at high potentials and that of NH_3 at lower potentials with N_2 formed at intermediate potentials. They also concluded that ammonia was the main product of the reduction of a NO adlayer. Whereas DEMS and RDE facilitate the identification of solution species formed and the reduction kinetics of solution NO, they are unable to provide direct information on the structures of surface NO compared with IRAS [15].

In contrast to intensive study by in situ IRAS on the adsorption and reduction of NO at other Pt-group metal electrodes, to the best of our knowledge no such report on a Ru electrode exists, and this is an interesting area of exploration. It has been reported that the surface states of a Pt-group metal electrode imposed a significant effect on the reduction of nitric oxide

* Corresponding author. Fax: +86 21 65641740.
E-mail address: wbcai@fudan.edu.cn (W.-B. Cai).

0021-9517/$ – see front matter
doi:10.1016/j.jcat.2007.05.006

[15,17]. A Ru electrode has a specific electronic effect, with a much stronger tendency to form an oxide layer on its surface in electrolytes compared with a Pt, Pd, or Rh electrode in practical applications [28–30]. The adsorption and reduction of NO can be expected to exhibit its own unique characteristics. In addition, previous in situ IRAS studies paid little attention to the time-resolved measurement on the reduction process of NO adlayers on related Pt-group electrodes [23], probably due to the restriction of the thin layer structure and relatively lower surface signals. Therefore, it is highly desirable to extract the relevant kinetic vibrational information on a Ru electrode for its potential application in electrocatalytic reduction of NO, NO_3^-, and NO_2^-. Fortunately, vibrational data for NO adlayers at Ru–UHV and Ru–gas interfaces obtained by EELS [9,10], HREELS [11], and IRAS [31–34] measurements can serve as good references for this purpose.

Surface-enhanced infrared absorption spectroscopy (SEIRAS) has been applied widely in surface science and electrochemistry because of its high signal sensitivity and simple surface selection rule [35–50]. In particular, SEIRAS in attenuated-total-reflection (ATR) configuration, (ATR-SEIRAS) is free from problems caused by thin layer structure, such as inhomogeneous current distribution and limited mass transport, and thus is favorable for real-time monitoring of adsorption and reaction at electrode surfaces [36–39]. Far less interference from bulk water signal in ATR-SEIRAS enables ready identification of vibrational bands at around 1600–1700 cm^{-1} without the need to use the effect of isotope shifts, which was once essential for IRAS study of NO adsorption and reaction at electrodes.

This work presents a real-time ATR-SEIRAS investigation of NO adsorption and reduction at a NO-predosed Ru electrode in 0.1 M $HClO_4$ (defined as case I), as well as a Ru electrode in 0.1 M $HClO_4$ + 20 mM $NaNO_2$ solution (defined as case II).

2. Experimental

A SEIRA-active Au nanoparticle film (ca. 60 nm thick) was coated on the total-reflecting plane of a hemicylindrical Si prism with an electroless plating method [45–48]. A Ru overlayer was electrodeposited onto the Au base film (working area, 1.33 cm^2) at −0.25 V for 600 s and then at −0.2 V for 900 s in a plating electrolyte containing 0.1 mM $RuCl_3$ and 0.5 M H_2SO_4, with a saturated calomel electrode (SCE) and a Pt mesh serving as the reference electrodes and counterelectrodes, respectively. In this way, a virtually pinhole-free Ru overlayer electrode can be obtained. The average mass thickness is calculated to be ca. 4.6 nm based on ICP-AES measurement. The average roughness factor is ca. 2.9, as estimated by electrochemical measurement in 0.1 M NaOH solution. (Details have been provided previously [45,46].) Ex situ AFM observation of the Ru nanofilm on a Si wafer was carried out with a Molecular Imaging Pico-SPM operated in the AC mode.

The NO-predosed Ru electrode was obtained by soaking the Ru nanofilm in a 0.1 M $HClO_4$ solution containing 20 mM $NaNO_2$ at open circuit potential for 1 min, followed by thorough rinsing with water [23]. This adlayer can be isolated because it resists a transfer to a nitrite-free solution [23]. The subsequent (spectro)-electrochemical measurements were performed in 0.1 M $HClO_4$ sparged with high-purity Ar. For comparison, corresponding measurements were also conducted for a bare Ru nanofilm electrode in 0.1 M $HClO_4$ containing 20 mM $NaNO_2$ or saturated NO, and similar results were obtained (not shown). A CHI 660B electrochemistry workstation was used for the potential-current control. All electrode potentials below are cited with a reversible hydrogen electrode (RHE) unless specifically addressed.

A Nicolet Magna-IR 760 FTIR spectrometer equipped with a liquid nitrogen-cooled MCT detector was used for real-time SEIRAS measurements and was operated at a resolution of 8 cm^{-1} with an acquisition time of 0.2 s (in case I) or 0.4 s (in case II) for each spectrum. In situ spectroscopy on Ru nanofilm electrodes were measured with the so-called Kretschmann ATR configuration (prism-thin metal film-solution geometry), as described in detail elsewhere [36]. Unpolarized infrared radiation from a ceramic source was focused at the interface by passing through the prism at the incident angle of ca. 65°, and the totally reflected radiation was detected. Real-time spectra were collected during the potential sweep from 0.8 to 0.0 V at 20 mV s^{-1} in case I and from 0.9 to 0.0 V then back to 0.9 V at 20 mV s^{-1} in case II. All of the spectra in this paper are shown in absorbance units defined as $-\log(I/I_0)$, where I and I_0 represent the intensities of the reflected radiation at the sample and reference potentials, respectively. All of the experiments were performed at room temperature.

3. Results and discussion

3.1. Voltammetric behavior

The nitrogen-containing species in the solution of 0.1 M $HClO_4$ and 20 mM $NaNO_2$ may consist of predominantly HNO_2 and bit of NO_2^- (hereinafter only HNO_2 is discussed for simplification), as well as trace amounts of NO and NO_3^- via disproportionation of partial HNO_2 [51,52], that is,

$$3HNO_2 \rightarrow NO_3^- + 2NO + H_3O^+. \quad (1)$$

It should be mentioned that this reaction is a slow process in the solution but is promoted in the presence of catalytic metal centers (e.g., Pt-group atoms) [52].

This property ensures the formation of saturated NO adlayer on a Ru electrode at the open circuit potential resembling that on other Pt-group metal electrodes, as revealed earlier by Ye et al. [51] and the Alicante group [20–23]. Fig. 1 shows cyclic voltammograms for a NO-predosed Ru electrode in deaerated 0.1 M $HClO_4$ (solid line) and a freshly electrodeposited Ru electrode in deaerated 0.1 M $HClO_4$ + 20 mM $NaNO_2$ solution (dashed line), respectively, with initial potentials near their open-circuit potentials (0.8 V for the former and 0.9 V for the latter). Also shown in Fig. 1 is the cyclic voltammogram for a Ru electrode in neat 0.1 M $HClO_4$ between 0.9 V and 0 V for comparison (dotted line). According to Colucci et al. [17], in the cathodic scan the very broad peak starting from ca. 0.50 V (RHE) for the NO-predosed Ru electrode in 0.1 M $HClO_4$ can

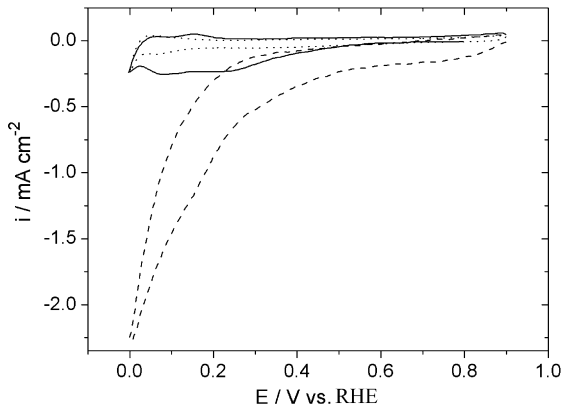

Fig. 1. Cyclic voltammogram (CV) of a Ru nanofilm electrode in 0.1 M $HClO_4$ (···), CV of a NO-predosed Ru nanofilm electrode in 0.1 M $HClO_4$ (—) and CV of a Ru nanofilm electrode in 0.1 M $HClO_4$ + 20 mM $NaNO_2$ (- - -). Scan rate: 20 mV s^{-1}.

be assigned to the slow reduction of ruthenium oxide, and the NO adlayer is not reduced in this potential region in the presence of the oxide. As the potential moved to a below ca. 0.3 V, additional reduction currents emerged due to the reduction of NO adlayer and the electrosorption of hydrogen [15,17]. The overall reduction reaction of NO adlayer at relative negative potentials can be represented simply as follows if NH_3 is assumed to be the main product (or NH_4^+ in the acid solution) [15], that is,

$$NO_{ads} + 6H^+ + 5e^- \rightarrow NH_4^+ + H_2O. \quad (2)$$

The subsequent cyclic voltammogram for the above Ru electrode is similar to that of a bare Ru electrode in 0.1 M $HClO_4$. A little difference is not surprising in consideration of the fact that a Ru electrode is very sensitive to its history and surface conditions [26]. Anyway, spectral evidence (vide infra) suggests that NO adlayer in case I can be reduced completely after the first segment potential scan.

In the case of the Ru electrode in 0.1 M $HClO_4$ + 20 mM $NaNO_2$ solution (dashed line), continuous NO supply to the Ru electrode can be achieved due to the catalytic decomposition of dissolved HNO_2 to NO, mimicking the situation of bubbling NO into 0.1 M $HClO_4$ (not shown here). During the cathodic scan, the HNO_2 can be reduced to form a series of products such as NO, N_2O, N_2, or NH_4^+ sequentially, depending on potentials applied, according to the report by Colucci et al. [17]. This may contribute to the much larger cathodic current observed for the Ru electrode in 0.1 M $HClO_4$ containing 20 mM $NaNO_2$. In particular, with gradual removal of the Ru oxide layer at the potentials below ca. 0.5 V, the reduction current began to increase. As the potential moved below 0.3 V, the cathodic current increased drastically, in response to electrocatalytic multiple-electron reduction of HNO_2 and NO (both solution and surface) into NH_4^+ [17].

Nevertheless, the overlapping of several reduction processes prevents the detailed revelation of specific information about reduction removal of the NO adlayer on Ru electrodes based on the above cyclic voltammograms [17]. In the next section, we apply in situ ATR-SEIRAS to provide insight into the spectral information of the structure and reduction of NO adlayers at Ru electrodes.

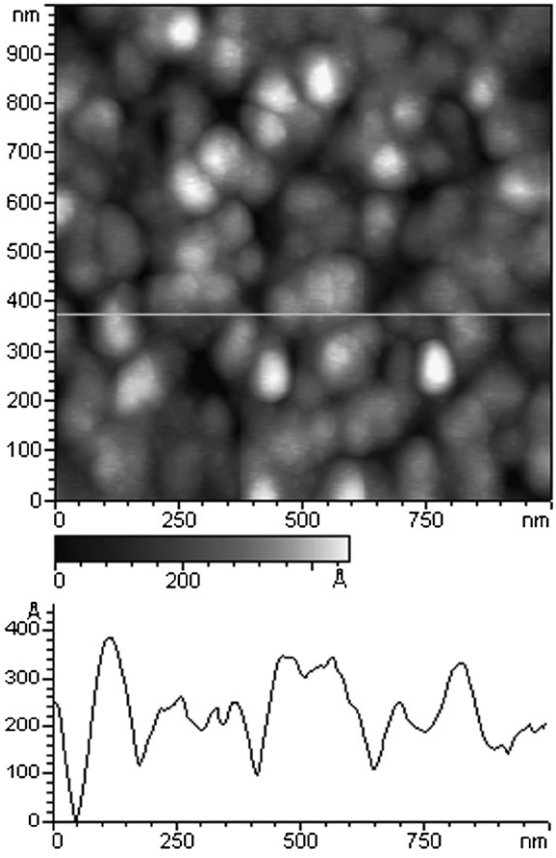

Fig. 2. Ex situ AFM image of a Ru nanofilm.

3.2. SEIRAS on a NO-predosed Ru electrode in 0.1 M $HClO_4$ (case I)

The morphology of the electrodeposited Ru nanofilm on an Au underlayer was characterized using ex situ AFM (Fig. 2), revealing that the Ru nanofilm consists of rather closely packed ellipsoidal particles. This island structure facilitates surface plasmon resonance under IR radiation to yield the SEIRA effect [37,45]. Theoretical calculations predict that nearly all metals can yield the SEIRA effect per se [36,37], without the need to borrow the SEIRA effect from underlying Au. Unlike SERS, in which a virtually "pinhole-free" metal layer with a few atomic layer thickness is required, the longer wavelengths of IR radiation allow for deposition of a much thicker Ru overlayer carry with SEIRA activity to ensure its "pinhole-free" feature [45,46,48].

The in situ time-resolved SEIRA spectra for the NO adlayer at the Ru electrode are shown in Fig. 3, which were collected in neat 0.1 M $HClO_4$ after isolation of the adsorbed NO preformed in 0.1 M $HClO_4$ + 20 mM $NaNO_2$ solution at the open-circuit potential for 1 min, the same pretreatment as for other Pt metal electrodes [20–23]. Series of spectra were collected during the potential sweep from 0.8 to 0.0 V at 20 mV s^{-1}, with an acquisition time of 0.2 s for each spectrum. The reference spectrum was taken at 0.0 V, at which NO was stripped off completely.

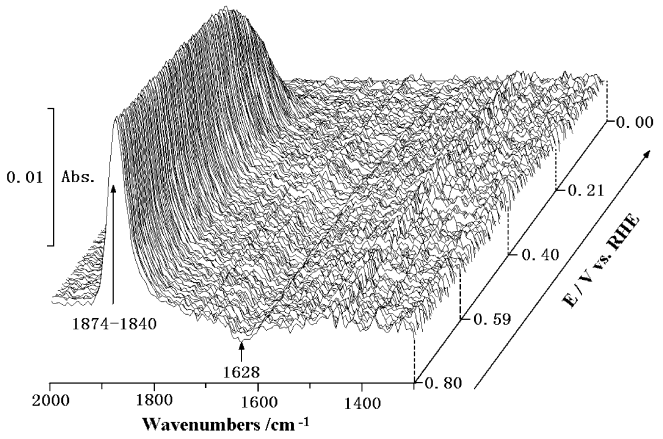

Fig. 3. Series of time-resolved ATR-SEIRA spectra of a NO-predosed Ru electrode in 0.1 M $HClO_4$ collected sequentially during a cathodic potential sweep from 0.8 to 0.0 V at 20 mV s^{-1}. The time resolution used and shown is 0.2 s. The reference spectrum was taken at 0.0 V. See the text for further details.

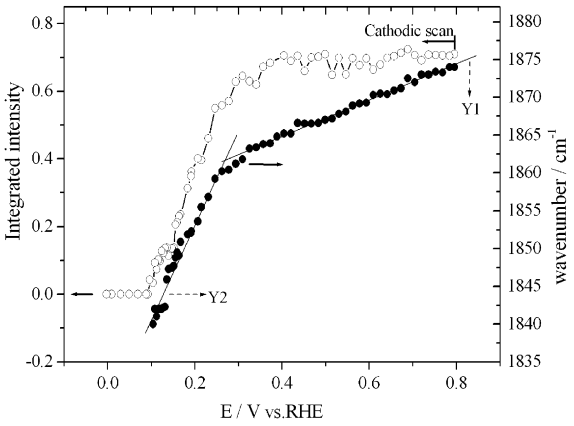

Fig. 4. Plots of the integrated IR band intensities (○) and the center frequency (●) of the ν_2(O)–NO band against the potential. Y1 and Y2 denote corresponding fitted lines. Data are adapted from Fig. 3.

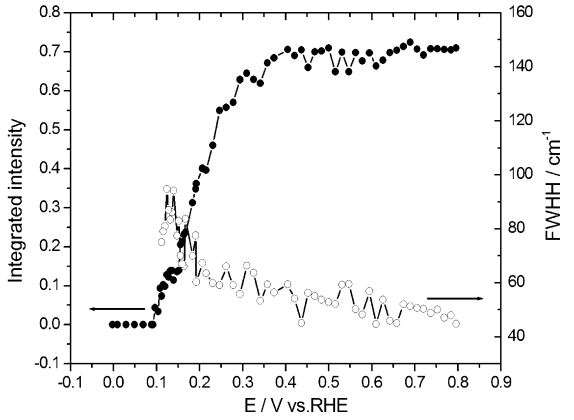

Fig. 5. Plots of the selected integrated IR band intensities (●) and full width at half height (FWHH) (○) of the ν_2(O)–NO band against the potential. Data are adapted from Fig. 3.

The electrodeposited Ru nanofilm is polycrystalline in nature with preferred Ru(001), whereas Ru(001) is the most stable and studied plane. Before analyzing the data in Fig. 3, it is helpful to briefly review the relevant results for the Ru–UHV or Ru–gas interface. Davydov and Bell [32] observed two bands for the N–O stretch, at 1880 cm^{-1} on the oxidized surface and at 1810 cm^{-1} on the reduced Ru surface with the transmission mode on supported Ru catalysts. Hayden et al. [31] assigned the band at 1780–1820 cm^{-1} at 85–130 K in UHV to the linear NO species adsorbed on clean Ru(001) surface (designated ν_2-NO species) and assigned the other band at 1846 cm^{-1} to linear NO species coadsorbed with oxygen atoms [designated ν_2(O)–NO species]. The geometrical structures of NO have been systematically studied on Ru(001) in UHV by TPD, IRAS, XPS, and LEED [33,34,53–55]. The main conclusions can be summarized as follows. At low temperature, the NO + O(2 × 1) configuration shows one IR band at ca.1610 cm^{-1}, assignable to the hcp-sited NO species [designated ν_1(O)–NO species], whereas the hcp-sited NO species on a clean Ru surface (designated ν_1-NO species) shows a band at ca.1504 cm^{-1}. On annealing at a higher temperature, the NO + O(2 × 1) configuration can convert to the NO + 2O(2 × 2) configuration, yielding a band at ca. 1860 cm^{-1} that can be ascribed to ν_2(O)–NO species.

The above structure-correlated vibrational information in the literature provides good references for the assignment of the bands observed here. Fig. 3 shows one band at 1874–1840 cm^{-1}, the frequency of which red-shifts during the cathodic potential sweep. Oxygen-containing species tend to form on a Ru electrode surface and cannot be reduced completely even in the low potential region of 0.3–0.1 V [28–30]. By recalling the vibrational data for the Ru–UHV or ambient–gas interface, this band can be reasonably assigned to NO linearly coadsorbed oxygen-containing species on Ru, that is, oxidized Ru sites [designated ν_2(O)–NO species for similarity] [32,33]. A weak and downward band at 1628 cm^{-1} can be assigned to δ_{HOH} of interfacial water [45], indicative of replacement of NO with H_2O on the Ru surface at lower potentials. However, multicoordinated NO species including ν_1(O)–NO species and ν_1-NO species were not detected in the whole potential range. Note also the absence of the bands for primary reduction products, such as NH_4^+ [23] at these lower potentials, suggesting a negligible adsorption, if any, for these soluble species.

Fig. 4 displays the plots of the integrated intensity (open circles) and the center frequency (filled circles) of the ν_2(O)–NO band as a function of potential. The band position versus potential plot can be separated into two linear parts, yielding slopes of 24 and 124 cm^{-1} V^{-1} for fitted lines Y1 and Y2, corresponding to potential ranges of approximately 0.8–0.3 V and 0.3–0.1 V. Fig. 5 shows the potential dependent band width (FWHH, open circles) and intensity (filled circles) for the ν_2(O)–NO band. The band intensity and width are nearly invariable from 0.8 to 0.3 V, suggesting that the NO adlayer is rather stable in this potential region. Thus, the increased cathode current response in Fig. 1 (solid line) as the potential was scanned from 0.8 to 0.3 V can be attributed to the slow partial reduction of surface oxide rather than to reduction of the NO adlayer. In addition, it can be inferred that such partial removal of surface oxide does not

result in a substantial change in the local environment for adsorbed NO molecules. Only at potentials below 0.3 V was obvious reduction of the ν_2(O)–NO species found, as evidenced by the significant decrease in band intensity and increase in band width (see Fig. 5). Nevertheless, NO molecules adsorbed on clean Ru sites (or ν_2-NO species) were not detected in the entire potential investigated. This suggests that the reduction of adsorbed NO molecules and their coadsorbed oxygen-containing species proceed simultaneously rather than separately, probably involving a hydrogenation step at these negative potentials [26]. In what follows we will treat these two species as a whole and designate them the ν_2(O)–NO species for convenience. All of the real-time SEIRAS results indicate that reduction of NO adlayer on a Ru electrode can proceed without the need for the complete removal of surface oxides, somewhat different from the previous assumption based merely on voltammetric measurement by Colluci et al. [17]. Because no bands (either unipolar or bipolar) for any surface NO species were detected over the potential range of 0.1–0.0 V in Figs. 3 and 4, complete reduction of the ν_2(O)–NO species can be deduced after the cathodic scan in case I. Again we demonstrated the importance of combined electrochemical and spectroscopic measurement in dealing with a complex electrochemical process.

It is interesting to note that the linear slope of Y2 line is much higher than that of Y1 in Fig. 4. For the former, in addition to the well-known Stark effect that may contribute to this linearity, the rapid concurrent movement of the ν_2(O)–NO species at the surface may be invoked to explain the larger slope. Ab initio density functional calculation indicates that NO on metal surfaces is highly mobile [14]. High mobility is assumed to also apply to the ν_2(O)–NO species on Ru, ensuring a rather uniform dilution of local ν_2(O)–NO species concentration in the process of reduction. The dilution of local coverage of ν_2(O)–NO species diminishes the dipole–dipole coupling effect and thus further decreases the νN–O frequency [56,57]. The rapid concurrent movement of the ν_2(O)–NO species facilitates the reduction of ν_2(O)–NO species occurring randomly throughout the layer and the rapid concurrent lowering of the coverage of NO, contributing to the larger slope of Y2.

3.3. SEIRAS on a Ru electrode in 0.1 M $HClO_4$ + 20 mM $NaNO_2$ (case II)

Fig. 6 shows series of SEIRA spectra collected during the initial cathodic potential scan from 0.9 to 0.0 V and then in the anodic potential scan back to 0.9 V at 20 mV s^{-1} on a Ru nanofilm electrode in 0.1 M $HClO_4$ containing 20 mM $NaNO_2$. The reference spectrum was taken at 0.0 V for Fig. 6a, in which the band located at 1886–1860 cm^{-1} in the cathodic scan or 1850–1870 cm^{-1} in the anodic scan can be assigned to the ν_2(O)–NO species [32,33]. The slight change in band position in the cathodic and anodic scans can be explained as a decrease in surface coverage in the latter. The other band located at 1530–1578 cm^{-1} in the cathodic scan or at 1520–1576 cm^{-1} in the anodic scan can be assigned to multicoordinated NO coadsorbed with oxygen-containing species [designated ν_1(O)–NO species] for it is accrete with ν_2(O)–NO species [33]. A very

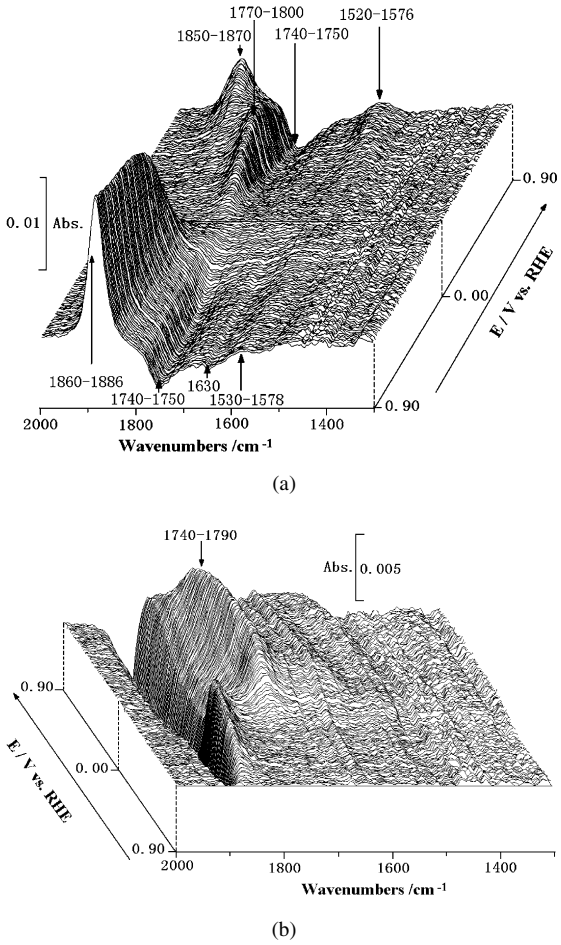

Fig. 6. Series of real-time SEIRA spectra collected at Ru nanofilm electrode/0.1 M $HClO_4$ + 20 mM $NaNO_2$ solution interface sequentially during a potential cycling sweep from 0.9 V to 0.0 V and then back to 0.9 V at 20 mV s^{-1}. The time resolution used and shown is 0.4 s. (a) The reference spectrum was taken at 0.0 V. (b) The reference spectrum was the first spectrum at 0.9 V.

weak and downward-directed band at 1630 cm^{-1} is assigned to δ_{HOH} of interface water at 0.0 V [45], as also detected in case I. Interestingly, a downward-directed band appeared at 1740–1750 cm^{-1} in the cathodic scan or at 1740–1800 cm^{-1} with a bipolar shape in the anodic scan. This band clearly was not detected in case I, suggesting that a new surface species was produced at lower potentials in case II.

To remove the bipolar band feature (related to the new species) in Fig. 6a for easy spectral analysis, the initial spectrum collected at 0.9 V was used as the reference to reconstitute the potential dependent series of spectra, as shown in Fig. 6b. In fact, a unipolar band at 1740–1790 cm^{-1} can be clearly identified. Careful examination reveals that this band is present in the low potential region from ca. 0.3 to 0.0 V in the cathodic scan and to ca. 0.7 V in the anodic scan. None of the following nitrogen-containing species may contribute to this band: HNO_2 (1670, 1275 cm^{-1}) [20], N_2O (2227, 1300 cm^{-1}), NH_4^+ (3040, 1680, 3145, 1400 cm^{-1}), NH_2 (matrix: 1500, 3220 cm^{-1}; surface: 3290, 1610, 3380 cm^{-1}), [NH_2^-] (3270, 1556, 3323 cm^{-1}), HNO (matrix: 3450, 1110, 1563 cm^{-1}), or NH_3 (3223, 1060, 3378, 1646 cm^{-1}) [58]. Based on the UHV

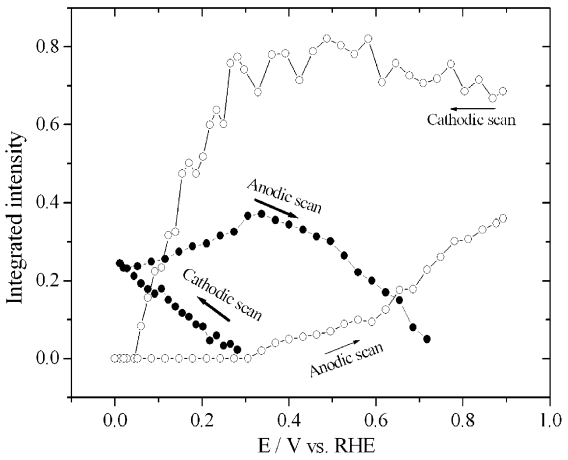

Fig. 7. Plots of the integrated intensities for the ν_2(O)–NO (○) and ν_2-NO (●) bands adapted from Fig. 6. See the text for details.

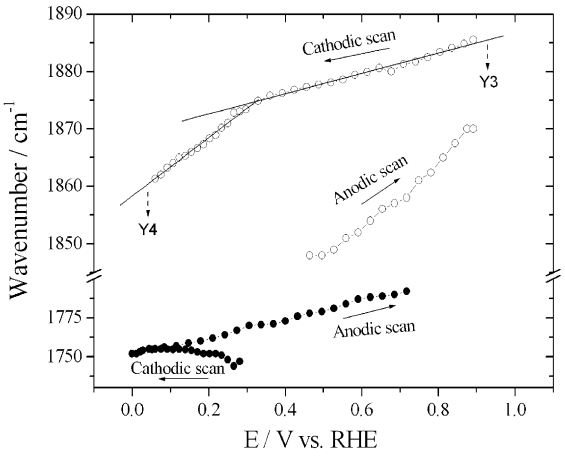

Fig. 8. Potential dependent center frequencies for the ν_2(O)–NO (○) and ν_2-NO (●) bands adapted from Fig. 6, as a function of potential. Y3 and Y4 denote corresponding fitted lines.

data reported by Hayden et al. [31], who detected a band at around 1780 cm^{-1} on clean surfaces of Ru (001) at 85 and 130 K for linearly adsorbed NO species, it is reasonable to assign the band observed at 1740–1790 cm^{-1} to NO linearly adsorbed on clean Ru sites rather than on oxidized Ru sites, that is, ν_2-NO species. The deviation of the center frequency from previous UHV data can be explained largely by the Stark effect and the solvent effect [59]. The assignment is further supported by potential dependent intensities for the ν_2(O)–NO and ν_2-NO bands, as shown in Fig. 7 (vide infra).

Fig. 7 shows the plots of selected integrated intensities of the ν_2(O)–NO bands (hollow circles) and the ν_2-NO bands (solid circles) against the potential. The plots of the center frequencies for the ν_2(O)–NO bands (hollow circles) and the ν_2-NO bands (filled circles) against the potential are displayed in Fig. 8. Y3 and Y4 denote fitted lines for the ν_2(O)–NO band frequency versus potential in the cathodic scan, showing slopes of 18 cm^{-1} V^{-1} for the potential range of 0.9–0.3 V and 51 cm^{-1} V^{-1} for the potential range of 0.3–0.05 V. These two values are smaller than their counterparts for the predosed NO adlayer on Ru electrode in Fig. 4. In addition, a somewhat higher local coverage of the oxygen-containing species or/and ν_2(O)–NO species on the Ru electrode can be reasonably expected in case II compared with case I, because a continuous NO supply from the solution to Ru surface in the former is maintained. That means that the higher the local coverage, the smaller the Stark tuning rate. A similar result also was found for CO adlayer on a Pt electrode [57]. The lower Stark tuning rate at a higher coverage may be explained by decreased d-π back-electron donation or partly screened local electric field due to intensified dipole–dipole coupling [56,57]. Nevertheless, two features similar to those shown in Fig. 4 are observed, consisting of the linearity of band frequency versus potential for the ν_2(O)–NO species during its reduction process (Y4) and the larger slopes for Y4 compared with Y3.

In the cathodic scan of Fig. 7, the ν_2(O)–NO band decreases sharply at potentials below ca. 0.3 V and loses its intensity completely at 0.05 V. In the meantime, the ν_2-NO band gains intensity steadily with subsequent cathodic and anodic potential scans until ca. 0.3 V. Fig. 7 also shows that starting at 0.35–0.8 V in the anodic scan, the ν_2-NO band decreases, accompanied by growth of the ν_2(O)–NO band, suggesting conversion of the ν_2-NO species to the ν_2(O)–NO species as a result of increased oxide formation at higher potentials.

The variation of the ν_2(O)–NO and ν_2-NO band intensities with potential in Fig. 7 may be envisioned as follows. The ν_2(O)–NO species began to be reduced at lower potentials in the cathodic scan. The presence of HNO_2 and NO in the solution shifted the complete reduction potential negatively from 0.1 V in case I to 0.05 V in case II. In the cathodic scan, the appearance of the ν_2-NO species at potentials below 0.3 V indicates that nominally reduced Ru sites began to form upon reduction of the ν_2(O)–NO species. As mentioned in case I, no ν_2-NO species was detected; thus, it was proposed that both NO and its environmental oxygen-containing species [or simplified as ν_2(O)–NO species] were reduced together when the potential was negatively scanned to 0.3 V and below. Therefore, the appearance and growth of the ν_2-NO species in the subsequent cathodic and anodic scans in case II can be attributed to readsorption of NO on the freshly formed nominal Ru sites. On one hand, more nominal Ru sites were reoccupied by NO molecules supplied by the continuous dissociation of HNO_2 in bulk solution and/or rapid reduction of adsorbed HNO_2 to form the ν_2-NO species as indicated in Eq. (1). On the other hand, the ν_2-NO species may undergo further reduction to NH_4^+ according to Eq. (2). The steadily increased band intensity for the ν_2-NO species from 0.3 to 0.0 V in the cathodic scan and then to ca. 0.3 V in the anodic scan suggests a gradually net accumulation of the ν_2-NO species before its conversion to the ν_2(O)–NO species at potentials above ca. 0.3 V, whereon the increase of the ν_2(O)–NO band was accompanied with the decrease of the ν_2-NO band. The zero intensity of the ν_2(O)–NO band from 0.1 to 0.3 V in the anodic scan suggests that the reformation of Ru oxides is negligible under current conditions.

4. Conclusion

In situ real-time ATR-SEIRAS in conjunction with cyclic voltammetry was applied to investigate the adsorption and reduction of nitric oxide at a Ru electrode in acidic solutions. For the NO-predosed Ru electrode in 0.1 M $HClO_4$ (case I), only atop NO coadsorbed with oxygen-containing species [namely, ν_2(O)–NO species] was detected. During the cathodic scan, the ν_2(O)–NO species began to be reduced at potentials below ca. 0.3 V. For the Ru electrode in 0.1 M $HClO_4$ + 20 mM $NaNO_2$ (case II), in addition to the dominant ν_2(O)–NO species, NO linearly adsorbed on nominal Ru sites (namely, ν_2-NO species) as well as multicoordinated NO coadsorbed with oxygen-containing species [namely, ν_1(O)–NO species] can be identified. No evidence was found for the conversion of ν_2(O)–NO to ν_2-NO species during its reduction; rather, the reverse process may occur at higher potentials. The net accumulation of the ν_2-NO species in case II resulted from the readsorption of NO on the nominally reduced Ru sites at lower potentials. In both cases, the ν_2(O)–NO species at Ru electrode can begin to be reduced without the need for complete removal of surface oxides.

Acknowledgments

This work was supported by the NSFC (grants 20473025, 20673027), SRFDP (grant 20040246008), NCET (grant 04-0349). Yan-Gang Yan was supported by the Innovation Fund of Fudan University (grant CQH 1615018). The authors thank Professor M. Osawa for providing the Si prisms.

References

[1] A.C.A. De Vooys , R.A. van Santen, J.A.R. van Veen, J. Mol. Catal. A 154 (2000) 203.
[2] W.J. Plieth, in: A.J. Bard (Ed.), Encyclopedia of Electrochemistry of the Elements, vol. 8, Marcel Dekker, New York, 1978, p. 321.
[3] G. Horanyi, E.M. Rizmayer, J. Electroanal. Chem. 188 (1985) 265.
[4] J.F. van der Plas, E. Barendrecht, Electrochim. Acta 25 (1979) 1463.
[5] I. Villegas, R. Gomez, M.J. Weaver, J. Phys. Chem. 99 (1995) 14832.
[6] M.J. Weaver, S. Zou, C. Tang, J. Chem. Phys. 111 (1999) 368.
[7] P. Hollins, Surf. Sci. Rep. 16 (1992) 53.
[8] M.T.M. Koper, R.A. van Santen, S.A. Wasileski, M.J. Weaver, J. Chem. Phys. 113 (2000) 4392.
[9] G.E. Thomas, W.H. Wienberg, Phys. Rev. Lett. 41 (1978) 1181.
[10] U. Schwalke, W.H. Weinberg, J. Vac. Sci. Technol. A 5 (1987) 459.
[11] K.M. Neyman, N. Rosch, K.L. Kostov, P. Jacob, D. Menzel, J. Chem. Phys. 100 (1994) 2310.
[12] F. Esch, S. Ladas, S. Kennou, A. Siokou, R. Imbihl, Surf. Sci. 355 (1996) L253.
[13] W.A. Brown, D.A. King, J. Phys. Chem. B 104 (2000) 2578.
[14] M. Gajdos, J. Hafner, A. Eichler, J. Phys. Condens. Matter 18 (2006) 13.
[15] A.C.A. De Vooys, M.T.M. Koper, R.A. van Santen, J.A.R. van Veen, J. Catal. 202 (2001) 387.
[16] G.E. Dima, A.C.A. De Vooys, M.T.M. Koper, J. Electroanal. Chem. 554–555 (2003) 15.
[17] J.A. Colucci, M.J. Foral, S.H. Langer, Electrochim. Acta 30 (1985) 1675.
[18] A.C.A. de Vooys, G.L. Beltramo, B. van Riet, J.A.R. van Veen, M.T.M. Koper, Electrochim. Acta 49 (2004) 1307.
[19] G.E. Dima, G.L. Beltramo, M.T.M. Koper, Electrochim. Acta 50 (2005) 4318.
[20] A. Rodes, V. Climent, J.M. Orts, J.M. Perez, A. Aldaz, Electrochim. Acta 44 (1998) 1077.
[21] A. Rodes, R. Gomez, J.M. Orts, J.M. Feliu, J.M. Perez, A. Aldaz, Langmuir 11 (1996) 3549.
[22] A. Rodes, R. Gomez, J.M. Perez, J.M. Feliu, A. Aldaz, Electrochim. Acta 41 (1996) 729.
[23] B. Alvarez, A. Rodes, J.M. Perez, J.M. Feliu, J.L. Rodriguez, E. Pastor, Langmuir 16 (2000) 4695.
[24] S. Zou, R. Gomez, M.J. Weaver, J. Electroanal. Chem. 474 (1999) 155.
[25] R. Gomez, M.J. Weaver, J. Phys. Chem. B 102 (1998) 3754.
[26] V. Rosca, G.L. Beltramo, M.T.M. Koper, Langmuir 21 (2005) 1448.
[27] G.L. Beltramo, M.T.M. Koper, Langmuir 19 (2003) 8907.
[28] M. Metikoš-Huković, R. Babić, F. Jović, Z. Grubač, Electrochim. Acta 51 (2006) 1157.
[29] S. Hadži-Jordanov, H. Angerstein-Kozlowska, M. Vuković, B.E. Conway, J. Phys. Chem. 81 (1977) 2271.
[30] S. Hadži-Jordanov, H. Angerstein-Kozlowska, M. Vuković, B.E. Conway, J. Electrochem. Soc. 128 (1978) 1471.
[31] B.E. Hayden, K. Kretzschmar, A.M. Bradshaw, Surf. Sci. 125 (1983) 366.
[32] A.D. Davydov, A.T. Bell, J. Catal. 49 (1977) 332.
[33] P. Jakob, M. Stichler, D. Menzel, Surf. Sci. 370 (1997) L185.
[34] H.J. Kreuzer, S.H. Payne, P. Jakob, D. Menzel, Surf. Sci. 424 (1999) 36.
[35] A. Hartstein, J.R. Kirtley, J.C. Tsang, Phys. Rev. Lett. 45 (1980) 201.
[36] M. Osawa, in: J.M. Chalmers, P.R. Griffiths (Eds.), Handbook of Vibrational Spectroscopy, vol. 1, Wiley, Chichester, 2002, p. 785.
[37] M. Osawa, Bull. Chem. Soc. Jpn. 70 (1997) 2861.
[38] B. Beden, C. Lamy, in: R.J. Gale (Ed.), Spectroelectrochemistry: Theory and Practice, Plenum Press, New York, 1988, chap. 5.
[39] R.J. Nichols, in: J. Lipkowski, P.N. Ross (Eds.), Adsorption of Molecules at Metal Electrodes, VCH, New York, 1992, chap. 7.
[40] T. Yajima, H. Uchida, M. Watanabe, J. Phys. Chem. B 108 (2004) 2654.
[41] M. Watanabe, Y.M. Zhu, H. Uchida, J. Phys. Chem. B 104 (2000) 1762.
[42] Y.X. Chen, A. Miki, S. Ye, H. Sakai, M. Osawa, J. Am. Chem. Soc. 125 (2003) 3680.
[43] M.-H. Shao, P. Liu, R.R. Adzic, J. Am. Chem. Soc. 128 (2006) 7408.
[44] A. Rodes, J.M. Orts, J.M. Pérez, J.M. Feliu, A. Aldaz, Electrochem. Commun. 5 (2003) 56.
[45] Y.-G. Yan, Q.-X. Li, S.-J. Huo, M. Ma, W.-B. Cai, M. Osawa, J. Phys. Chem. B 109 (2005) 7900.
[46] Y.-G. Yan, Q.-X. Li, S.-J. Huo, Y.-N. Sun, W.-B. Cai, Acta Chim. Sinica 63 (2005) 545.
[47] M. Ma, Y.-G. Yan, S.-J. Huo, Q.-J. Xu, W.-B. Cai, J. Phys. Chem. B 110 (2006) 14911.
[48] S.-J. Huo, X.-K. Xue, Y.-G. Yan, Q.-X. Li, M. Ma, W.-B. Cai, Q.-J. Xu, M. Osawa, J. Phys. Chem. B 110 (2006) 4162.
[49] T. Wandlowski, K. Ataka, S. Pronkin, D. Diesing, Electrochim. Acta 49 (2004) 1233.
[50] S. Pronkin, T. Wandlowski, Surf. Sci. 573 (2004) 109.
[51] S. Ye, H. Kita, J. Electroanal. Chem. 346 (1993) 489.
[52] W.J. Plieth, in: A.J. Bard (Ed.), Encyclopedia of the Electrochemistry of the Elements, vol. 8, Marcel Dekker, New York, 1978, chap. 5.
[53] M. Stichler, D. Menzel, Surf. Sci. 391 (1997) 47.
[54] E. Umbach, S. Kulkarni, P. Feulner, D. Menzel, Surf. Sci. 88 (1979) 65.
[55] M. Stichler, D. Menzel, Surf. Sci. 419 (1999) 272.
[56] D.K. Lambert, Electrochim. Acta 41 (1996) 623.
[57] S.-C. Chang, M.J. Weaver, J. Chem. Phys. 92 (1990) 4582.
[58] K. Nakamoto, Infrared and Raman Spectra of Inorganic and Coordination Compounds, fifth ed., Wiley, New York, 1997.
[59] N. Kizhakevariam, I. Villegas, M.J. Weaver, J. Phys. Chem. 99 (1995) 7677.